Simulation of vacuum membrane distillation process for desalination with Aspen Plus

Wensheng Cao [a,c,d], Iqbal M. Mujtaba [b,*]

[a] College of Mechanical and Energy Engineering, Jimei University, Xiamen 361021, China

[b] School of Engineering and Informatics, University of Bradford, West Yorkshire, Bradford BD7 1DP, UK

[c] Fujian Province Key Lab of Energy Cleaning Utilization and Development, Jimei University, China

[d] Cleaning Combustion and Energy Utilization Research Center of Fujian Province, Jimei University, China

* Corresponding author. E-mail address: I.M.Mujtaba@bradford.ac.uk (Prof. I.M. Mujtaba).

Abstract

This paper presents a simulation study of vacuum membrane distillation (VMD) for desalination. A simulation model was built on Aspen Plus® platform as user defined unit operation for VMD module. A simplified mathematical model was verified and the analysis of process performance based on simulation was also carried out. Temperature and concentration polarization effects are significant in the conditions of higher feed temperature and/or vacuum pressure. The sign of $(P_{I,f} - P_{I,p})$, difference of the vapour pressures between at the membrane interfaces, is a pointer of the vacuum pressure threshold. Increasing the vacuum pressure at lower feed temperature is an effective way to increase the permeate flux and reduce the energy consumption simultaneously.

Keywords:

Vacuum membrane distillation; Desalination; Process simulation; Heat and mass transfer

1. Introduction

Vacuum membrane distillation (VMD) is a promising technology for the aqueous solutions treatments which have been fallen into three main processes: the single component, the binary components and the multicomponent transport process. The applications of these processes consist of desalination, concentration, and extraction of organics and dissolved gases from water. In terms of economic and safety considerations, VMD is capable of competing with other well-established separation technologies [1].

In VMD configurations, transport mechanisms of vapor molecules across the membranes are described by some models such as dusty-gas model [2-4] and Schofield's model [2], Ballistic model [5], Monte Carlo model [6], velocity slip model

[7] and ANN model [8], including one-dimensional [9,10] and two-dimensional models [11]. These models can be brought into commercial process simulators by developing user-defined modules [12].

Most of the simulation softwares such as Aspen Plus, Aspen HYSYS, PRO/II and ChemCAD can satisfy the research needs of design, simulation and optimization [13]. The membrane models must consist of the operation parameters of the process, such as temperatures, pressures, compositions, membrane area, transport properties, and configuration, etc. But these process simulation softwares lack independent and intrinsic models of membrane unit for gas or liquid separations. Nevertheless, the process simulators do have the merits of ideal computing environments for performing phase equilibrium, material balance and energy balance calculations requested by membrane models. Simulation softwares are provided with large databases of physical and thermodynamic properties for predicting unknown physicochemical properties with regard to any gas or liquid phase mixtures [14]. Rautenbach et al. [12] designed and performed simulations of membrane plants in Aspen Plus. Chang et al. [15] presented two simulations of membrane distillation modules for desalination by developing user's model on Aspen Plus platform. Guan et al. [16] conducted an evaluation of hollow fiber-based direct contact and vacuum membrane distillation systems using aspen process simulation.

This study intends to build the model for VMD desalination module on Aspen Plus® platform considering the heat and mass transfer resistances. Aspen Plus allows users to link into the Excel spreadsheet software application to enhance its modeling capabilities. In this paper, a User2 unit operation block in Aspen Plus simulation with an Excel spreadsheet to perform the calculation of the membrane model was employed as a unit operation in a process simulation and participated wholly in the overall material and energy balance calculations of a larger process.

2. Mathematical models

The permeate flux assesses the VMD separation performance can be obtained

$$J = \frac{m_p}{A_m \cdot t} \qquad (1)$$

where J denotes the permeate flux, m_p is the mass of the permeate, A_m is the membrane area and t is the operation time.

For non-volatile solutes dissolved in the aqueous solutions, the rejection (R) of the solutes can be expressed

$$R = \frac{c_f - c_p}{c_f} \times 100 \qquad (2)$$

where c_f is the concentration of solute in the feed and c_p is the concentration of solute in the permeate.

2.1 Heat transfer

Membrane distillation (MD) is a phase-change evaporation and transportation process. Generally, the heat transfer of MD includes three steps: convection heat transfer in the feed boundary layer, conduction heat transfer through the membrane and the heat flows together with the vapour through the membrane pores, i.e. the latent heat of vaporization, and convection heat transfer in the permeate boundary layer. At steady state, the overall heat transfer coefficient (H) of the MD process can be expressed in the resistance series [17, 18]

$$\frac{1}{H} = \frac{1}{h_f} + \frac{1}{h_m + \frac{J \cdot \Delta H_v}{\Delta T_m}} + \frac{1}{h_p} \qquad (3)$$

where h_f is the individual heat transfer coefficient of the feed, h_m is the individual heat transfer coefficient of the membrane and h_p is the individual heat transfer coefficient of the permeate; ΔH_v is the heat of vaporisation and ΔT_m is the temperature difference across the membrane.

For VMD, the heat transfer resistance on the permeate side can be neglected compared to the other resistances for the vacuum pressure is applied on the permeate side of the membrane [19, 20]. The heat transfer resistance in the feed relies on experimental hydrodynamics and thermodynamics and it is changed with the feed flow rate of the corresponding feed temperature. The membrane resistance relies on the membrane parameters like thickness, pore size, porosity and tortuosity, etc [1].

In the porous membrane, heat is transferred together with the mass flux across the membrane pores and by conduction through the membrane material and the vapour that trapped inside the pores. The heat transfer through the membrane (Q_m) is given by

$$Q_m = J \cdot \Delta H_v + \frac{k_m}{\delta_m}(T_{I,f} - T_{I,p}) \qquad (4)$$

where k_m is the membrane thermal conductivity and δ_m is the thickness; $T_{I,f}$ and $T_{I,p}$ are the temperatures of membrane interfaces on the feed and permeate side,

respectively. The thermal conductivities of the polymers used to fabricate the MD membranes such as the polypropylene (PP), polyethylene (PE), polytetrafluoroethylene (PTFE) and polyvinylidene fluoride (PVDF) range from 0.15 to 0.51 W/m K. Because the MD operates at temperatures between 20 and 100 °C, the thermal conductivities of the water vapour vary from 0.019 to 0.024 W/m K, while the air ranging from 0.025 to 0.032 W/m K. Along with the membrane porosity is typically between 35 and 76%, the thermal conductivities of the membranes can be cut down to 0.04~0.06 W/m K [21]. The vacuum pressure applied on the permeate side of the membrane can remove the water vapour and the air from the membrane pores during the VMD process, so the thermal conductivities of the VMD membranes are further decreasing. The conduction heat transfer through the VMD membranes are usually omitted as a result [22-24]

$$Q_m = J \cdot \Delta H_v \qquad (5)$$

The heat transfer across the boundary layer in the feed often limits the permeate flux because a larger quantity of heat must be supplied to the membrane interface to vaporise the liquid. The convection heat transfer (Q_f) in the feed boundary layer can be given [25, 26]

$$Q_f = h_f (T_{b,f} - T_{I,f}) \qquad (6)$$

where $T_{b,f}$ is the bulk temperature on the feed side.

The heat transfer coefficient can be obtained from the corresponding Nusselt number

$$Nu = \frac{h_f \cdot d_h}{k_f} \qquad (7)$$

where d_h is the hydraulic diameter of the feed flow channel and k_f is the feed thermal conductivity.

d_h is calculated from the Reynolds number (Re) and and k_f is calculated from Prandtl number (Pr) defined as respectively

$$\mathrm{Re} = \frac{v \cdot d_h \cdot \rho}{\mu} \qquad (8)$$

$$\mathrm{Pr} = \frac{c_p \cdot \mu}{k_f} \qquad (9)$$

where v is the velocity, ρ is the density, μ is the viscosity and c_p is the heat

capacity. The empirical correlations among Nu, Re and Pr numbers are diverse in terms of various types of VMD membrane modules. Different membrane modules will have the different hydrodynamics on the feed side and thus varying the heat transfer performance, such as inside/out hollow fibre module and outside/in hollow fibre module. A simple form of the Nusselt empirical equation is proposed by [25]

$$Nu = a \cdot \mathrm{Re}^{b} \cdot \mathrm{Pr}^{c} \qquad (10)$$

where *a*, *b* and *c* are characteristic constants of concerning the module design and feed flow regime. Table 1 describes equation (10) for different hollow fibre modules of VMD.

(Table 1)

2.2 Mass transfer

The transport of a volatile component in the VMD process can be fallen into three steps: firstly the component diffuses out of the feed bulk to reach the membrane surface; secondly the component vaporises at the vapour–liquid (V-L) interface and transfers through the membrane pores; and last diffuses in the vacuum permeate side. The overall mass transfer coefficient (K) can be expressed by resistance series [27]

$$K = \frac{1}{\kappa_f} + \frac{1}{\kappa_m} + \frac{1}{\kappa_p} \qquad (11)$$

where κ_f is the individual mass transfer coefficient of the feed, κ_m is the individual mass transfer coefficient of the membrane and κ_p is the individual mass transfer coefficient of the permeate. The vacuum applied on the permeate side of the membrane can increase the diffusion coefficient and the mass transfer resistance on the permeate side can be neglected compared to the other mass transfer resistances [27].

In the MD process, the volatile component passes through the gas-phase membrane pores. On the basis of the Darcy's law, the flux (J) is proportional to the vapour pressure difference (ΔP) across the membrane [28]

$$J = C \cdot \Delta P = C(P_{I,f} - P_{I,p}) \qquad (12)$$

where *C* is the membrane permeability, $P_{I,f}$ is the vapour pressure at the membrane surface on the feed side and $P_{I,p}$ is the vapour pressure at the membrane surface on the permeate side.

For the single component transport process, the water partial pressure has been similar to the Raoult's law by supposing that the solutions are ideal diluted solutions [29]

$$P_w = x_w \cdot P_w^o \qquad (13)$$

where x_w is the water fraction and P_w^o is the saturated water vapour pressure.

The water saturation pressure can be calculated from the Antoine equation [30]

$$P_w^o = \exp\left[23.1964 - \frac{3816.44}{T - 46.13}\right] \qquad (14)$$

Mass transfer across the porous membrane is formed by three basic mechanisms: Knudsen diffusion, viscous flow and molecular diffusion. Any coalescent of the mechanisms is possible in the MD processes. Knudsen number ($\mathrm{K}n$) is a pointer to decide the operative mechanism under given experimental process conditions in a given pore diameter. The Knudsen number is defined as

$$\mathrm{K}n = \frac{\lambda}{d_p} \qquad (15)$$

where λ is the mean free path of the molecule and d_p is the pore diameter of the membrane.

While $\mathrm{K}n > 10$, the Knudsen diffusion will be the prevailing mechanism of the mass transfer. The membrane permeability can be defined as [31-33]

$$C_{\mathrm{K}n} = \frac{2}{3}\left(\frac{8M_i}{\pi RT}\right)^{\frac{1}{2}} \frac{\varepsilon r}{\delta \tau} \qquad (16)$$

where M_i is the molecular weight of the transporting component *i*, R is the gas constant and T is the temperature; ε is the porosity, r is the pore radius, δ is the thickness and τ is the pore tortuosity of the membrane.

Table 2 shows the mean free path of water vapour molecules at a permeate pressure of 1000Pa in case of the water vapour pressure at the V-L interface equals the saturated vapour pressure.

(Table 2)

The mass transfer across the boundary layer on the feed side would restrict the permeate flux when using the relatively high permeable membranes in the VMD process. The mass balance in the feed is described by the film theory [35-37]

$$J_i = \kappa_f \cdot c_f \cdot \ln\left(\frac{x_{i,I} - x_{i,p}}{x_{i,b} - x_{i,p}}\right) \qquad (17)$$

where $x_{i,b}$ is the fraction of the transporting component *i* in the bulk feed, $x_{i,p}$ is the fraction of the transporting component *i* in the permeate and $x_{i,I}$ is the fraction of the transporting component *i* at the membrane interface on the feed side.

The mass transfer coefficient can be obtained from the corresponding Sherwood number

$$Sh = \frac{\kappa_f \cdot d_h}{D_f} \qquad (18)$$

where D_f is the diffusion coefficient in the feed solution. The Schmidt number (Sc) can be defined as

$$Sc = \frac{\mu}{\rho_f \cdot D_f} \qquad (19)$$

A simple empirical equation of the relation of Sherwood number and Schmidt number is expressed

$$Sh = a \cdot \mathrm{Re}^b \cdot Sc^c \qquad (20)$$

It may be difficult to express the formula of Eq. (20). The possible solution of it is to propose an analogy between heat and mass transfer processes [38]

$$Nu \cdot Sc^{-c} = Sh \cdot \mathrm{Pr}^{-c} \qquad (21)$$

Table 3 describes equation (20) for different hollow fibre modules of VMD.

(Table 3)

3. Simulation

In order to simplify the mathematical models it is necessary to make the following assumptions concerning the nature of the process:

(a) The resistances of heat transfer in the feed and permeate, as well as the thermal conductivity of the membrane, were neglected.

(b) The resistances of mass transfer in the feed and permeate were considered to be negligible.

(c) The Knudsen diffusion dominated the process of mass transfer.

(d) Temperature polarisation coefficient ($TPC = \frac{T_{I,f}}{T_{b,f}}$) $\rightarrow$ 1, for the case where the heat transfer resistance in the liquid feed phase was negligible.

(e) Concentration polarisation coefficient ($CPC = \frac{c_{b,f}}{c_{I,f}}$) $\rightarrow$ 1, for the case where the mass transfer resistance in the feed phase couldn't control the process.

The simulated flow chart of VMD process was presented in Fig. 1. The HEATX is a built-in heat-exchanging unit in Aspen plus, while the MEMBRANE is a User2 unit with an Excel spreadsheet.

(Figure 1)

The structural parameters of the VMD membrane used for simulation were summarized in Table 4.

(Table 4)

The VMD process requires the energy for feed solution pumping/circulating, heating and operating the vacuum pumps. The energy utilised for heating the feed solution occupies the largest fraction, which is greater than 90% of the total energy consumption of the VMD system [39, 40]. In order to simplify the process the pumps and the condenser were omitted in Figure 1.

Aspen Plus offers several interfaces for including custom or proprietary models in Aspen Plus simulations. Among these is the option to use a User2 unit operation block in an Aspen Plus simulation with an Excel spreadsheet to perform the calculations.

First use Aspen Plus to build a process flowsheet, specify feed and product streams, and enter real and integer parameters corresponding to the membrane. Then use Excel to create a spreadsheet to calculate product stream properties. Aspen Plus will write data to and read data from the Excel spreadsheet. Table 5 and 6 are Aspen steams and blocks inputs, respectively.

(Table 5)

(Table 6)

4. Results and discussion

4.1 Model verification for VMD

For verifying the models, the simulation results were compared to the experimental results. Figure 2 shows the schematic diagram of the experimental

system [41]. A cross flow VMD module made from the Tianjin Hydroking Science and Technology Ltd (China) was employed in the experiment (Tab. 2). An acid washing loop shown as dotted line for membrane cleaning was included in the VMD system.

(Figure 2)

Parts of the data are shown in Figure 3~5. For VMD, the simplified model is capable of predicting the experimental results, although there are differences between the model predicated water fluxes and the experimental data.

(Figure 3)

Figure 3 shows the comparisons of measured (*Experiment*) and simulated (*Simulation*) permeate fluxes with feed temperature. It can be seen that the gap of fluxes between them grows with increased feed temperature, although the trend is similar. The relative errors at different temperatures were -45%, 11%, 25% and 48% orderly. This is due to the fact that the temperature polarization effect increases with the feed temperature. The temperature at the membrane surface reduces significantly when working at higher feed temperatures because larger heat of vaporisation is required to increase the mass flux. The effect of the feed temperature is also more significant on the concentration polarization.

Both temperature and concentration polarization effects, i.e. the heat and mass transfer resistances in the liquid phase, are significant with the feed temperature, i.e. TPC $\rightarrow$ 0 and CPC $\rightarrow$ 0. The heat and mass transfer resistances, which depend on different designs of VMD modules and operation conditions, are the rate limiting step for a high-flux condition because they will delay the heat and mass across the boundary layer in the liquid feed phase and thus reduce the permeate flux. The operation conditions include feed flow rate and feed concentration. At the higher flow rates, the heat and mass transfer coefficients in the liquid feed phase increase because the temperature and concentration at the membrane surface respectively approach to the corresponding temperature and concentration in the bulk phase, resulting in the higher fluxes. Also, the water vapour flux generally decreases when the feed concentration increases due to the reduction in the partial pressure of water as a result of the activity coefficient of water decreases and the presence of the concentration polarization.

The effects of temperature and concentration polarization can also be seen from Figure 4 and 5 at higher vacuum pressure. From Fig. 4~5, it can be observed that the flux is more sensitive to the permeate pressure. In other words, the permeate pressure is an effective parameter to affect the flux.

(Figure 4)

(Figure 5)

The comparisons of experimental and simulated permeate fluxes with vacuum pressure at T_f = 60°C and 70°C are shown in Fig. 4~5. There is an interesting phenomena that the permeate flux rises very slightly at lower vacuum pressure, but when vacuum pressure is higher than a certain value, the flux tends to rise sharply. Kuang et al [42] attributed the phenomena to the vaporization behavior change of the hot-side solution from surface evaporation to intense boiling, but Wang et al [41] rejected this explanation. As can be seen from the simulation lines, the red points of lower flux values before sharply rising remain zero flux in the simplified model simulation. This is because in these red points cases, the vapour partial pressure at the membrane surface on the feed side is less than the pressure on the permeate side, i.e. $(P_{I,f} - P_{I,p}) < 0$. When the vacuum pressure is more than a certain value $[(P_{I,f} - P_{I,p}) > 0]$, the water permeate flux will increase significantly. So the sign of $(P_{I,f} - P_{I,p})$ can be a pointer of the vacuum pressure threshold. When the sign of $(P_{I,f} - P_{I,p})$ is positive, the permeate flux rises drastically.

Moreover, the simulation results by an Artificial Neural Network (ANN) based model [8] using the same experimental data can be observed in Figs. 3~5. They are in agreement with the experimental data because the ANN model was set up based on the experimental data to describe the performance behaviours of the VMD process. However, certainly the predictions by the ASPEN PLUS maintain similar trends to those by experiments and by ANN model. Therefore, we believe the ASPEN based simulation can be used for further performance evaluation of the VMD process. ANN based model would be restrictive to this effect.

To handle start-up/shut-down operations of VMD process related to the frequent maintenance of the membranes, the model should be modified according to the operation. The start-up operation includes system inspection, opening the electric

heater, opening the magnetic pump, filling the condenser with condensed water, opening the vacuum pump and fresh water collection in order. The shut-down operation consists of closing the electric heater, closing the vacuum pump, vacuum tank exhaust, closing the magnetic pump and closing the condensed water in order. To be sure, there should be a membrane cleaning after a limited time of device running. The consideration of start-up/shut-down operations is about process dynamic simulation involving the operation parameters variation with time during the process running from start-up to shut-down.

4.2 Process performance

In Fig. 6, the relationship among temperatures of feed, x-out, retentate and permeate is presented. From this it can be seen that with the rise of the feed temperature, the x-out temperature decreases to transfer more heat energy to the feed. The permeate temperature maintains a horizontal line for the vacuum pressure of permeate side keeping a constant value of 0.088MPa. The temperature of the vacuum side of the membrane can be considered approximately equal to $T_{I,p}$ and it can be estimated by the Antoine equation [43, 44]. Although a larger quantity of heat is supplied to the membrane interface to vaporise the liquid, the retentate temperature almost equals the corresponding feed temperature (very slightly less than the latter) at the condition of 110 L/h total flow.

(Figure 6)

Fig. 7 shows the simulated variation of permeate flux versus vacuum pressure at different feed temperatures. It can be seen that the permeate flux increases with the rising of feed temperature and vacuum pressure, and the lines at different feed temperatures remain parallel to each other. The permeate flux is proportional to the vacuum pressure at a certain feed temperature. According to Figure 7 there is a regular interaction effect between the feed inlet temperature and the vacuum pressure, and they are the main factors influencing the permeate flux of process performance index.

(Figure 7)

Our analysis also revealed that the permeate rate with varying vacuum pressure at different feed temperatures (Figure 8) has the same certain law with Fig. 7 as the permeate rate and the permeate flux only has a difference of membrane area times. Both of them are associated with the specific energy consumption.

(Figure 8)

The specific energy consumption (for heating the feed solution) with varying vacuum pressure at different feed temperatures is shown in Figure 9. Careful comparison among the three lines reveals that the energy consumption decreases with the rise of vacuum pressure and feed temperature, and it falls more rapidly with increased vacuum pressure at lower feed temperature. For example, increasing the vacuum pressure from 0.078 to 0.083 MPa at T_f = 65^{o}C, there was a sharp fall of energy consumption from 20920 to 2935 kWh/m^3. It also works at T_f = 60^{o}C, the energy consumption drops from 16434 to 2508 kWh/m^3 with varying the vacuum pressure from 0.083 to 0.088 MPa. At higher feed temperature, for instance T_f = 70^{o}C, the energy consumption stays low from 2867 to 890 kWh/m^3 with the variation of the vacuum pressure from 0.078 to 0.093 MPa. Because the energy utilised for heating the feed solution accounts for more than 90% of the total energy consumption of the VMD system, it is an effective way to increase the vacuum pressure at lower feed temperature for achieving lower energy consumption.

(Figure 9)

Most of the VMD systems are provided with high thermal energy consumption and very low recovery ratio of water production. By recycling the concentrated brine as feed, or using free heating resources such as waste heat or solar/geothermal energy can remarkably reduce the total energy requirement.

5. Conclusions

Vacuum membrane distillation is a promising technology for the sake of aqueous solutions treatment such as desalination. The mechanisms of VMD process mainly comprise heat transfer across the membrane and on the feed side, and mass transfer across the membrane and on the feed side. Aiming at establishing a quick approach to predict the key output parameters associated with VMD module performance and process efficiency, Aspen plus was employed to conduct systematic evaluation with a user-defined subroutine model. A simplified mathematical model of the heat and mass transfer was developed and compiled as user customized unit to simulate the hollow

fibre-based VMD module. The unit operations directly have access to the intrinsic simulation software models for physicochemical properties and thermodynamics through the stream parameters and flash calculations.

The mathematical model was verified by comparing the simulation results with the experimental data and the ANN model from literatures. The analysis of process performance based on simulation was carried out. Both temperature and concentration polarization effects on the permeate flux are significant in the conditions of higher feed temperature and/or higher vacuum pressure. The sign of $(P_{I,f} - P_{I,p})$ is a pointer of the vacuum pressure threshold, where the permeate flux rises drastically when $(P_{I,f} - P_{I,p}) > 0$. The specific energy consumption for heating the feed solution is very high due to very low recovery ratio. Increasing the vacuum pressure at lower feed temperature is an effective way to increase the permeate flux and reduce the energy consumption simultaneously.

Acknowledgements

The author is extremely grateful to the University of Bradford, as well as the 2013 Visiting Scholar Program of Fujian Province in China, which supported the author (conferred the title of Honorary Visiting Academic) to research at the University of Bradford. This paper was financially supported by the Huang Huizhen Discipline Construction Foundation of Jimei University (ZC2012015) and the Technology Project of Fujian Provincial Department of Education (JA12191). This work was also supported by the Technology Project of State Administration of Work Safety (201310180001), and the Guiding Project (the former Key Project) of Fujian Provincial Department of Science & Technology.

Nomenclature

J Permeate flux, kg/m^{2}s

m Mass, kg

A Area, m^2

t Time, s

R Rejection, % or Gas constant, J/mol K

c Concentration, mol/L

H Overall heat transfer coefficient, W/m^{2}K

h Individual heat transfer coefficient, W/m^{2}K

ΔH_v Heat of vaporization, J/kg

T Temperature, K

Q Heat flux, W/m^2

k Thermal conductivity, W/m K

Nu Nesselt number

d Diameter, m

Re Reynolds number

v Velocity, m/s

Pr Prandtl number

c_p Heat capacity, J/kg K

K Overall mass transfer coefficient, m/s

κ Individual mass transfer coefficient, m/s

C Membrane permeability, kg/m^{2}s Pa

P Vapour pressure, Pa

P_v Vacuum pressure or vacuum degree, Pa

P^o Saturation vapour pressure, Pa

x Fraction in liquid phase

Kn Knudsen number

M Molecular weight, kg/mol

r Pore radius, m

Sh Sherwood number

D Diffusivity, m^2/s

Sc Schmidt number

Subscript

m membrane

p permeate or pore

f feed

I membrane interface

h hydraulic

w water

Greek letters

δ Thickness, m

ρ Density, kg/m^3

μ Viscosity, Pa s

λ Mean free path, m

ε Porosity

τ Tortuosity

References

[1] Chiam C., Sarbatly R., Vacuum membrane distillation processes for aqueous solution treatment—A review, Chemical Engineering and Processing 74 (2013) 27–54.

[2] Shao F., Hao C., Ni L., Zhang Y., Du R., Meng J., Liu Z., Xiao C., Experimental and theoretical research on N-methyl-2-pyrrolidone concentration by vacuum membrane distillation using polypropylene hollow fiber membrane, Journal of Membrane Science 452 (2014) 157–164.

[3] Fan H., Peng Y., Application of PVDF membranes in desalination and comparison of the VMD and DCMD processes, Chemical Engineering Science 79 (2012) 94–102.

[4] Woods J., Pellegrino J., Burch J., Generalized guidance for considering pore-size distribution in membrane distillation, Journal of Membrane Science 368 (2011) 124–133.

[5] Soukane S., Chelouche S., Naceur M.W., A ballistic transport model for vacuum membrane distillation, Journal of Membrane Science 450 (2014) 397–406.

[6] Imdakm A.O., Khayet M., Matsuura T., A Monte Carlo simulation model for vacuum membrane distillation process, Journal of Membrane Science 306 (2007) 341–348.

[7] Ramon G., Agnon Y., Dosoretz C., Heat transfer in vacuum membrane distillation: Effect of velocity slip, Journal of Membrane Science 331 (2009) 117–125.

[8] Khayet M., Cojocaru C., Artificial neural network modeling and optimization of desalination by air gap membrane distillation, Separation and Purification Technology 86 (2012) 171–182.

[9] Lee J., Kim W., Numerical modeling of the vacuum membrane distillation process, Desalination 331 (2013) 46–55.

[10] Shim S.M., Lee J.G., Kim W.S., Performance simulation of a multi-VMD desalination process including the recycle flow, Desalination 338 (2014) 39–48.

[11] Zuo G., Guan G., Wang R., Numerical modeling and optimization of vacuum membrane distillation module for low-cost water production, Desalination 339 (2014) 1–9.

[12] Rautenbach R., Knauf R., Struck A. Vier J., Simulation and design of membrane plants with AspenPlus, Chem. Eng. Technol. 19 (1996) 391–397.

[13] Chowdhury M. H. M., Simulation, design and optimization of membrane gas separation, chemical absorption and hybrid processes for CO_2 capture, Doctor Dissertation in Chemical Engineering of Waterloo Ontario Canada 2011.

[14] Davis R. A., Simple gas permeation and pervaporation membrane unit operation models for process simulators, Chem. Eng. Technol. 25 (2002) 717–722.

[15] Chang H., Liau J., Ho C., Wang W., Simulation of membrane distillation modules for desalination by developing user's model on Aspen Plus platform, Desalination 249 (2009) 380–387.

[16] Guan G., Yang X., Wang R., Field Robert, Fane Anthony G., Evaluation of hollow fiber-based direct contact and vacuum membrane distillation systems using aspen process simulation, Journal of Membrane Science 464 (2014) 127–139.

[17] Khayet M., Godino P., Mengual J. I., Theory and experiments on sweeping gas membrane distillation, J. Membr. Sci. 165 (2000) 261–272.

[18] Termpiyakul P., Jiraratananon R., Srisurichan S., Heat and mass transfer characteristics of a direct contact membrane distillation process for desalination, Desalination 177 (2005) 133–141.

[19] Khayet M., Khulbe K. C., Matsuura T., Characterization of membranes for membrane distillation by atomic force microscopy and estimation of their water vapour transfer coefficients in vacuum membrane distillation process, J. Membr. Sci. 238 (2004) 199–211.

[20] Izquierdo-Gil M. A., Abildskov J., Jonsson G., The use of VMD data/model to test different thermodynamic models for vapour–liquid equilibrium, J. Membr. Sci. 239 (2004) 227–241.

[21] Khayet M., Membranes and theoretical modeling of membrane distillation: a review, Adv. Colloid Inter. Sci. 164 (2011) 56–88.

[22] Mericq J. P., Laborie S., Cabassud C., Vacuum membrane distillation of seawater reverse osmosis brines, Water Res. 44 (2010) 5260–5273.

[23] Fan H., Peng Y., Application of PVDF membranes in desalination and comparison of the VMD and DCMD processes, Chem. Eng. Sci. 79 (2012) 94–102.

[24] Wang H., Li B., Wang L., Song S., Wang J., Feng Y., Wang S., Permeate flux curve characteristics analysis of cross-flow vacuum membrane distillation, Ind. Eng. Chem. Res. 51 (2012) 487–494.

[25] Qi B., Li B., Wang S., Investigation of shell side heat transfer in cross-flow designed vacuum membrane distillation module, Ind. Eng. Chem. Res. 51(2012) 11463–11472.

[26] Lovineh S. G., Asghari M., Rajaei B., Numerical simulation and theoretical study on simultaneous effects of operating parameters in vacuum membrane distillation, Desalination 314 (2013) 59–66.

[27] Khayet M., Matsuura T., Preparation and characterization of polyvinylidene fluoride membranes for membrane distillation, Ind. Eng. Chem. Res. 40 (2001) 5710–5718.

[28] Lawson K. W., Lloyd D. R., Membrane distillation, J. Membr. Sci. 124 (1997)1–25.

[29] Banat F., Al-Asheh S., Qtaishat M., Treatment of waters colored with methylene blue dye by vacuum membrane distillation, Desalination 174 (2005)87–96.

[30] Fan H., Peng Y., Application of PVDF membranes in desalination and comparison of the

VMD and DCMD processes, Chem. Eng. Sci. 79 (2012) 94–102.

[31] Khayet M., Khulbe K. C., Matsuura T., Characterization of membranes for membrane distillation by atomic force microscopy and estimation of their water vapour transfer coefficients in vacuum membrane distillation process, J. Membr. Sci. 238 (2004) 199–211.

[32] Mengual J. I., Khayet M., Godino M. P., Heat and mass transfer in vacuum membrane distillation, Int. J. Heat Mass Transfer 47 (2004) 865–875.

[33] Alkhudhiri A., Darwish N., Hilal N., Membrane distillation: a comprehensive review, Desalination 287 (2012) 2–18.

[34] Sun A. C., Kosar W., Zhang Y., Feng X., Vacuum membrane distillation for desalination of water using hollow fiber membranes, Journal of Membrane Science 455 (2014) 131–142.

[35] Mericq J. P., Laborie S., Cabassud C., Vacuum membrane distillation of seawater reverse osmosis brines, Water Res. 44 (2010) 5260–5273.

[36] Soni V., Abildskov J., Jonsson G., Gani R., Modelling and analysis of vacuum membrane distillation for the recovery of volatile aroma compounds from black currant juice, J. Membr. Sci. 320 (2008) 442–455.

[37] Mericq J. P., Laborie S., Cabassud C., Evaluation of systems coupling vacuum membrane distillation and solar energy for seawater desalination, Chem. Eng. J. 166 (2011) 596–606.

[38] Gryta M., Concentration of NaCl solution by membrane distillation integrated with crystallisation, Sep. Sci. Technol. 37 (2002) 3535–3558.

[39] Sarbatly R., Chiam C. K., Evaluation of geothermal energy in desalination by vacuum membrane distillation, Appl. Energy 112 (2013) 737–746.

[40] Wang X., Zhang L., Yang H., Chen H., Feasibility research of potable water production via solar-heated hollow fibre membrane distillation system, Desalination 247 (2009) 403–411.

[41] Wang Yongqing, Xu Zhilong, Lior Noam, Zeng Hui, Experimental investigation of a solar thermal-driven vacuum membrane distillation desalination system, Proceedings of ECOS 2013.

[42] Kuang Q., Li L., Min L., et al, Desalination of Luobupo bitter and salty water by vacuum membrane distillation, Membrane Science and Technology 27 (4) (2007) 46–49 (In Chinese).

[43] Lovineh S. G., Asghari M., Rajaei B., Numerical simulation and theoretical studyon simultaneous effects of operating parameters in vacuum membrane dis-tillation, Desalination 314 (2013) 59–66.

[44] Zhang J., Li J.-D., Duke M., Hoang M., Xie Z., Groth A., Tun C., Gray S., Modelling of vacuum membrane distillation, J. Membr. Sci. 434 (2013) 1–9.

[45] Li B., Sirkar K. K., Novel membrane and device for vacuum membranedistillation-based desalination process, J. Membr. Sci. 257 (2005) 60–75.

[46] Sarti G. C., Gostoli C., Bandini S., Extraction of organic components from aque-ous streams

by vacuum membrane distillation, J. Membr. Sci. 80 (1993) 21–33.

[47] Bandini S., Saavedra A., Sarti G. C., Vacuum membrane distillation: experi-ments and modelling, AlChE J. 43 (1997) 398–408.

[48] Bandini S., Gostoli C., Sarti G. C., Separation efficiency in vacuum membranedistillation, J. Membr. Sci. 73 (1992) 217–229.

[49] Bandini S., Sarti G. C., Heat and mass transport resistances in vacuum membrane distillation per drop, AlChE J. 45 (1999) 1422–1433.

Table 1. Nusselt empirical equations of heat transfer across feed boundary layers [1]

Nu equations	Description	Hollow fibre module
$Nu = 1.86(\mathrm{Re}\,\mathrm{Pr}\,d_h / L)^{1/3}$	Re < 2100	Inside/out [40, 45]
$Nu = 3.66 + \frac{0.0668(\mathrm{Re}\,\mathrm{Pr}\,d_h / L)}{1+0.045(\mathrm{Re}\,\mathrm{Pr}\,d_h / L)^{2/3}}$	Constant wall temperature; Laminar flow	Inside/out [46]
$Nu = 1.04\,\mathrm{Re}^{0.4}\,\mathrm{Pr}^{0.36}(\frac{\mathrm{Pr}}{\mathrm{Pr}_w})^{0.25} F_c$	10 < Re < 500	Outside/in [24, 45]

Table 2. Mean free path of water vapour molecules [34]

T (^{o}C)	30	40	50	60	70	80
λ (μm)	3.65	3.45	3.40	3.40	3.44	3.50

Table 3. Sherwood empirical equations of mass transfer across feed boundary layers [1]

Sh equations	Description	Hollow fibre module
$Sh = 1.62(\mathrm{Re}\,Scd_h / L)^{1/3}$	Laminar flow	Inside/out [47]
$Sh = 3.66 + \frac{0.0668(\mathrm{Re}\,Scd_h / L)}{1+0.045(\mathrm{Re}\,Scd_h / L)^{2/3}}$	Constant wall temperature; Laminar flow	Inside/out [48]
$Sh = 0.023\,\mathrm{Re}^{0.8}\,Sc^n$	Re > 10000	Inside/out [49]

Table 4. Characteristics of the hollow fiber membrane

Membrane (PP)	Effective area (m^2)	Porosity	Pore radius (μm)	Thickness (μm)	Tortuosity
Hollow fibre	0.25	0.55	0.1	220	2

Table 5. Aspen streams input

State variables	FEED-HEA	X-IN
Temperature (^{o}C)	25	80
Pressure (kPa)	120	120
Total flow (L/h)	110	110
Mass-Conc (gm/L)	35	1E-7

Table 6. Aspen blocks input

HEATX	Arrangement/Range
Flow direction	Countercurrent
Cold stream outlet temperature (^{o}C)	60~70
Cold side outlet pressure (kPa)	110
Hot side outlet pressure (kPa)	110

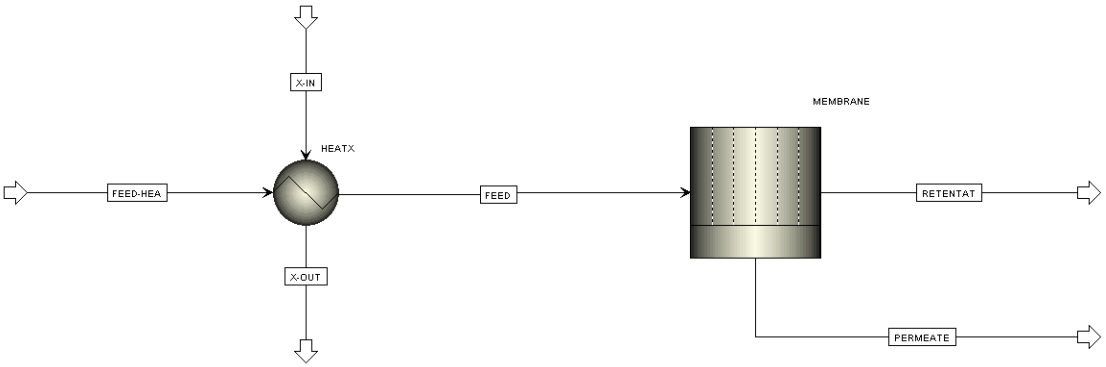

Figure 1. Flow sheet of VMD process in Aspen simulation

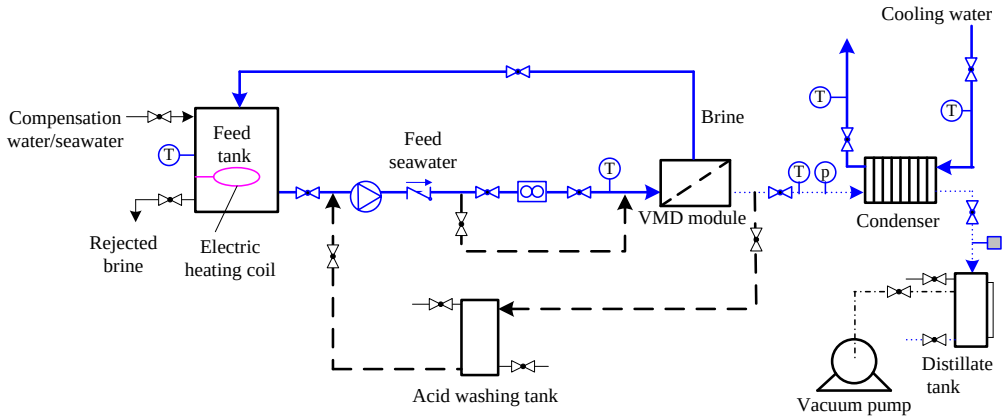

Figure 2. VMD experimental set-up in Jimei University [41]

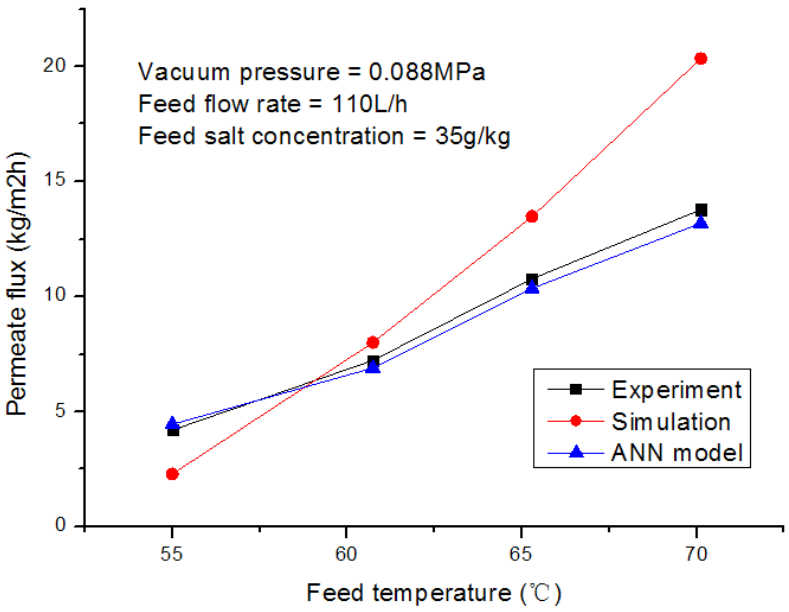

Figure 3. Model verification of permeate flux vs. feed temperature

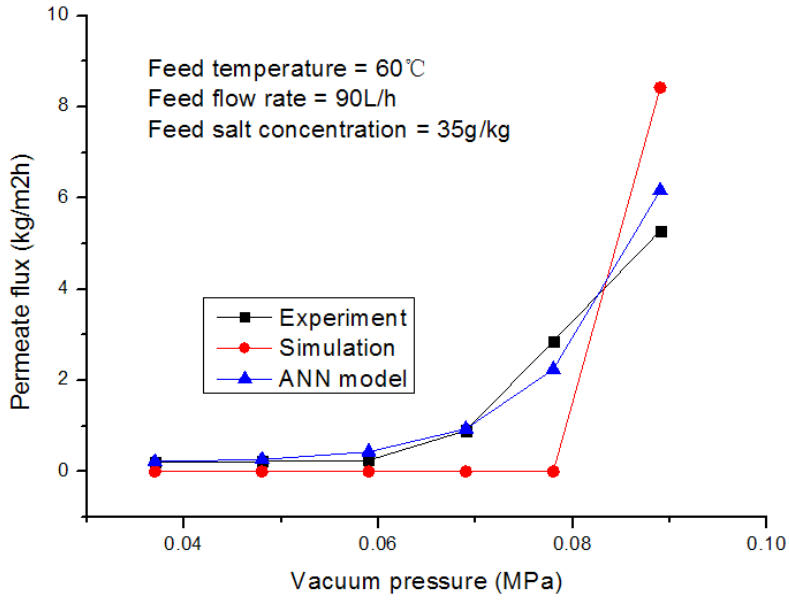

Figure 4. Model verification of permeate flux vs. vacuum pressure (T_f = 60°C)

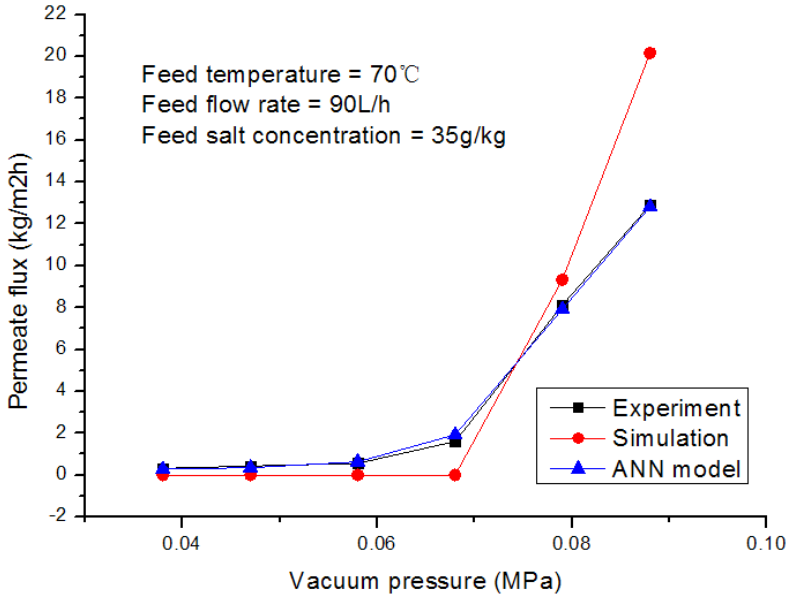

Figure 5. Model verification of permeate flux vs. vacuum pressure (T_f = 70°C)

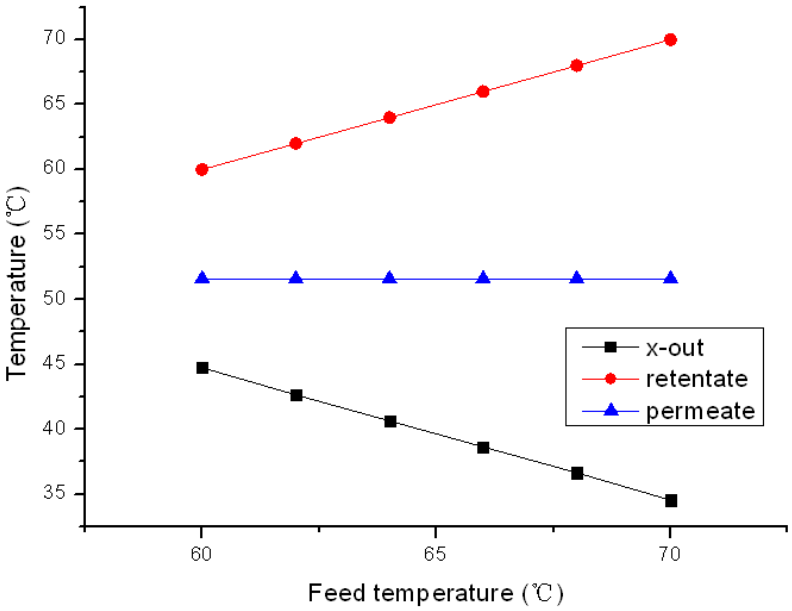

Figure 6. Relationship among temperatures of feed, x-out (HEATX hot stream outlet), retentate and permeate

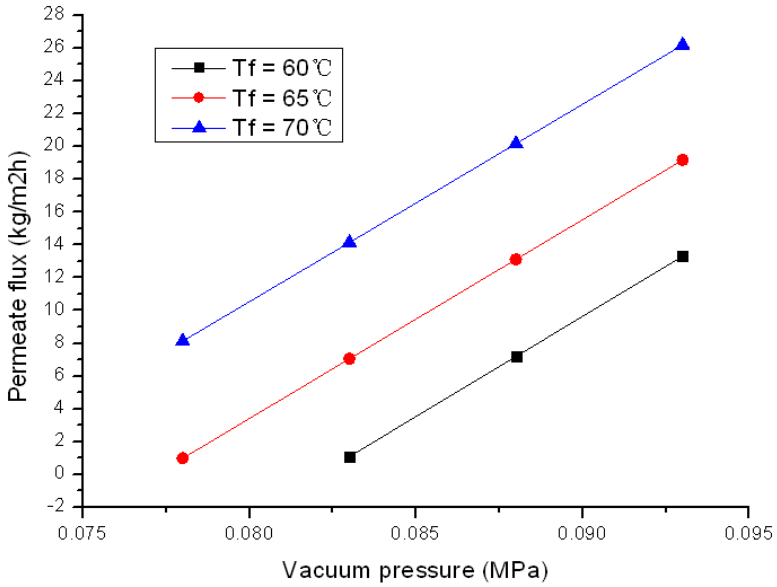

Figure 7. Variation of permeate flux versus vacuum pressure at different feed temperatures

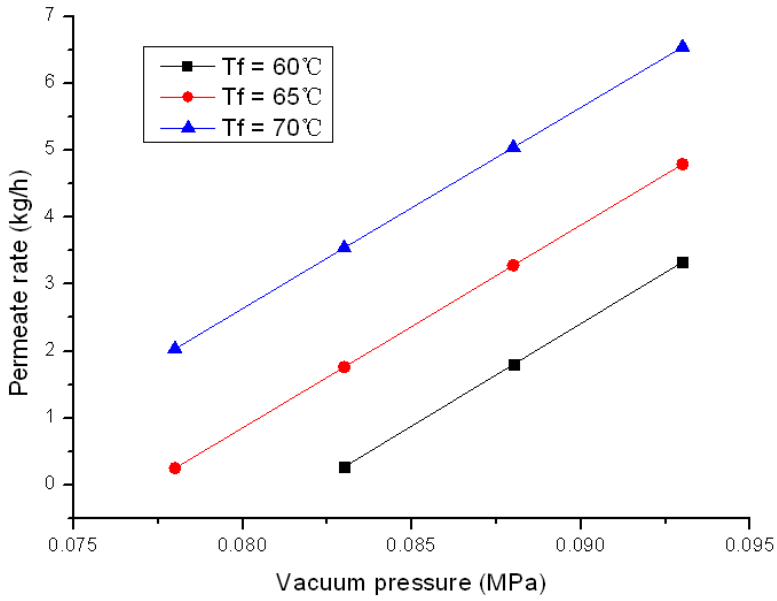

Figure 8. Permeate rate with varying vacuum pressure at different feed temperatures

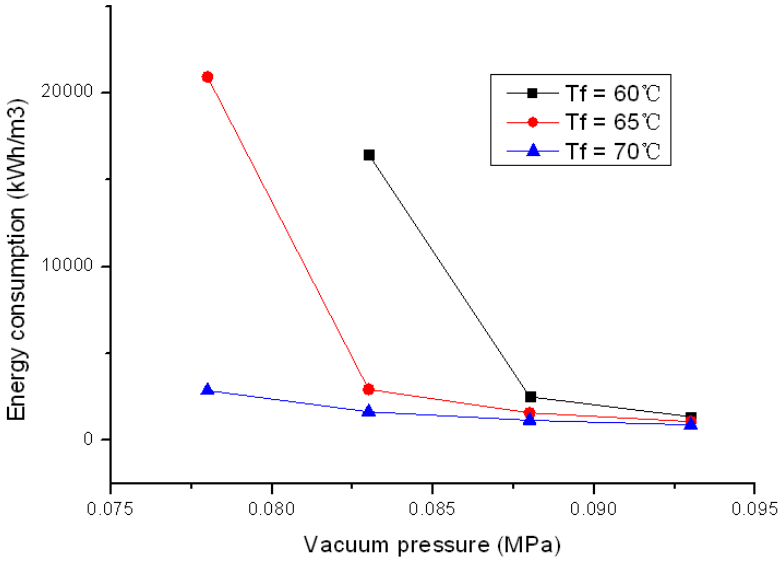

Figure 9. Specific energy consumption with varying vacuum pressure at different feed temperatures

List of Tables

List of Figures